Avalanche-mode Si light-emitting transistor for narrow-band emission near 760 nm

Dutta, Satadal; Hueting, Raymond J.E.; Verbiest, Gerard J.

DOI
10.1109/LED.2022.3200349

Publication date
2022

Document Version
Final published version

Published in
IEEE Electron Device Letters

Avalanche-Mode Si Light-Emitting Transistor for Narrow-Band Emission Near 760 nm

Satadal Dutta, Raymond J. E. Hueting, *Senior Member, IEEE*, and Gerard J. Verbiest

***Abstract*— We report an avalanche-mode light-emitting transistor (AMLET) in silicon (Si), based on a lateral bipolar junction, which emits light near 760 nm optical wavelength with a record low bandwidth of 38 nm. The AMLET, designed in a CMOS-compatible silicon-on-insulator (SOI) photonics platform, is optically confined within a 0.21 μm thick SOI layer, which forms a Fabry-Pérot (FP) resonator perpendicular to the Si surface. Light is emitted from the reverse biased emitter-base junction via phonon-assisted hot carrier recombination and, additionally, minority carriers are injected via the forward-biased Base-Collector junction. The combination of injection from collector terminal through a narrow base and FP optical resonance, yields a high optical power efficiency of 4.3×10^{-6} at $V_{BC} = 0.8$ V and $V_{EB} = 10$ V. Our work opens new possibilities in spectral-engineering of Si light-emitters, which could boost performance of all-Si optical interconnects and sensors.**

***Index Terms*— Avalanche breakdown, electroluminescence, Fabry-Pérot resonance, integrated optics, silicon.**

I. Introduction

SILICON (Si) p-n junctions exhibit broad-band electroluminescence (EL) at wavelengths $\lambda \sim$ 400–900 nm when operated in avalanche-mode (AM), with low efficiencies [1], [2], [3], [4]. Driven by the success of CMOS technology, the advent of Si photonics, and a growing demand for increased on-chip functionality, research on Si light-sources has gained attention [5], [6], [7], [8], [9], [10], [11], [12]. The AM-EL of Si has a significant spectral overlap with the responsivity of Si photodiodes [7], [13], with the range of human vision [14], and with the absorption spectrum of various biochemical entities [15], [16]. As such, despite the low optical power efficiency ($\eta_{opt} \sim 10^{-6}$), AM Si LEDs have successfully emerged as light-sources in monolithic optical interconnects [5], [8], [17], pigment sensors [18], and CMOS micro-displays [11]. The performance metrics in such end-applications, e.g. energy consumption per bit [8], [19] and sensor detection threshold [20], [21], [22], benefit from an increased η_{opt} in a wavelength-range of interest.

Manuscript received 11 August 2022; accepted 17 August 2022. Date of publication 19 August 2022; date of current version 27 September 2022. This work was supported by the Plantenna Research Programme through the 4TU Federation, The Netherlands. The review of this letter was arranged by Editor S. Zhang. *(Corresponding author: Satadal Dutta.)*

Satadal Dutta and Gerard J. Verbiest are with the Department of Precision and Microsystems Engineering, Delft University of Technology, 2628 CD Delft, The Netherlands (e-mail: s.dutta-1@tudelft.nl).

Raymond J. E. Hueting is with the Electrical Engineering, Mathematics and Computer Science (EEMCS) Faculty, University of Twente, 7522 NB Enschede, The Netherlands.

Color versions of one or more figures in this letter are available at https://doi.org/10.1109/LED.2022.3200349.

Digital Object Identifier 10.1109/LED.2022.3200349

Aided by several commercially available CMOS technologies, significant efforts have been made to increase η_{opt} and to stimulate the AM EL-intensity in a narrow bandwidth. These include carrier injection in a 3-terminal device [4], carrier energy and momentum engineering [23], [24], increasing field-profile uniformity via superjunction LEDs [25], and gated FET-based LEDs [11], [26]. Here, we present an avalanche-mode light-emitting transistor (AMLET) fabricated in a CMOS-compatible Si-photonics platform, that implements the electronic functionality of a lateral bipolar junction (inspired by [4], [28]) within an optically confined SOI-cavity, to enhance AM EL within a record-low bandwidth and high η_{opt}.

II. Results and Discussion

The AMLET design consists of a lateral n-p-n bipolar junction with symmetrically doped emitter (E), base (B) and collector (C) regions. The base length is 1.0 μm, while the total device length is 21.0 μm (Fig. 1(a)). Two n-p-n device units are connected in parallel with a shared base electrode. Highly doped n^+/p^+ implants form ohmic contacts to bond pads for biasing. Fig. 1(b) shows the cross-section of the AMLET fabricated in the iSiPP50G technology [27] from IMEC without any process modification. The nominal Si layer thickness is 0.22 μm, which reduces to $t_{Si} =$ 0.21 μm post-fabrication. The Si device is etched all around. The total junction area parallel to the y-z plane is $2t_{Si} \cdot 10 \approx 4.2$ μm^2. Fig. 1(c) shows the TCAD simulated electric field profile $F(x)$ along the E-B ($x = 0$) and B-C junction ($x = 1$ μm) using the ATLAS device simulator [29]. ATLAS solves Poisson equation coupled with drift-diffusion and continuity equations, while the Selberherr impact-ionization model [30] was employed to simulate avalanche breakdown.

The AMLET was measured in continuous dc-operation at 298 K in common-base configuration (Fig. 1(d)) with the E-B junction set in AM. The E and C terminals were biased, respectively, under a fixed voltage bias and a fixed current bias via a Keysight B2912A precision SMU. The AM EL spectral irradiance $\varepsilon(\lambda)$ was measured by mounting a lensed multi-mode optical fiber pigtail of an LWP lightwave probe vertically. The LWP probe was fed to an AvaSpec ULS2048CL-EVO spectrometer. Total optical power P_{opt} was obtained by integrating $\varepsilon(\lambda)$ over the λ-range 450–1000 nm and calibrating ε at a given λ using an AvaLight-DH-S-BAL light-source and a ThorLabs S155C photoreceiver (connected to PM100 power meter). Figs. 1(e), (f) show, respectively, the top-view die micrograph and the AM EL micrographs of

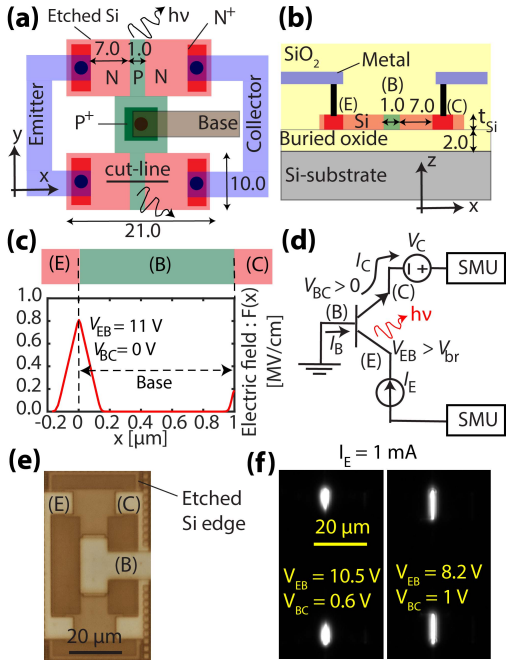

Fig. 1. Schematic (a) layout and (b) device cross-section of the AMLET, fabricated in iSiPP50G technology [27], with complete Si etch around it for optical confinement. Indicated dimensions in panels (a) and (b) are in μm. (c) TCAD simulated 1-D electric-field profile along the cut-line (shown in (a)) of the AMLET with symmetric doping levels, at V_{EB} = 11 V. (d) Schematic common-base biasing scheme used to measure light-emission from the AM E-B junction. (e) Top-view die micrograph and (f) EL-micrograph of the AMLET, captured with 20 s integration time for the indicated biases.

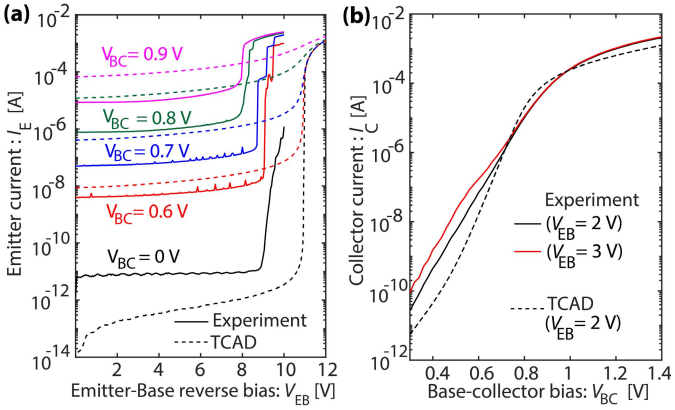

Fig. 2. Measured and TCAD simulated [29] I-V curves showing (a) avalanche breakdown of the E-B junction for varying B-C junction forward bias V_{BC}, and (b) forward-biased I_C-V_{BC} characteristics with V_{EB} = 2 V (black) and 3 V (red).

the AMLET for both low and high injection from the B-C junction, captured with a CS165MU digital camera; the latter with a 20 s integration time. We observe that high injection increases the spatial uniformity in the light-emission along the y-axis.

The measured I_E-V_{EB} characteristics (see Fig. 2(a)) exhibits a breakdown voltage $V_{br} \approx 10$ V, for $V_{BC} = 0$ V. As the forward bias V_{BC} increases, the injected minority carriers in the base region increase, thereby increasing I_E by several orders of magnitude. The same trend is obtained using TCAD I-V characteristics, where the current and carrier densities

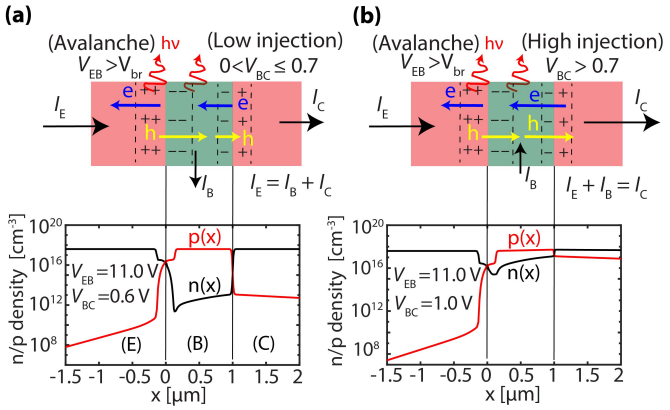

Fig. 3. Schematic (top) illustration of the AMLET operation, and (bottom) TCAD simulated 1-D electron/hole density profiles with E-B junction in avalanche for cases: (a) low injection (V_{BC} = 0.6 V), and (b) high injection (V_{BC} = 1.0 V) from forward biased B-C junction. The blue, yellow and black arrows represent flow of electrons, holes and total current through the terminals, respectively.

are simulated along the x-axis (1-D) assuming a uniform doping level of 4×10^{17} cm^{-3} (to fit simulations), and a carrier recombination lifetime of 2.5 ns. The discrepancies between TCAD and experiments are likely due to non-uniform doping depth-profiles in the experimental material, which could activate a parasitic transistor in parallel [31], as can be noticed from the kink in the forward biased I_C-V_{BC} characteristics (Fig. 2(b)) at $V_{BC} \approx 0.6$ V, showing a ~10 times higher measured current at low injection compared with TCAD. V_{BR} decreases (from 10 V to 8 V in experiment) with inreasing V_{BC}, indicating a clear injection-level dependency of carrier multiplication.

For optical measurements, we set $V_{EB} > V_{br}$ (Fig. 1(d)). The E-B junction emits light (Fig. 1(f)), at I_E = 1 mA, for an increasing V_{BC} in steps from 0 to 1 V. The AMLET operation is governed by field-driven impact ionization in the E-B junction and carrier injection via diffusion current through the narrow base. For $V_{BC} \leq 0.7$ V, injection from the B-C junction is low, as shown in Fig. 3(a). Hot electrons (holes) generated in the E-B junction due to avalanche multiplication are swept to the emitter (base) by the high electric field (see Fig. 1(c)). The net I_B flows out of the terminal: only a small fraction of holes are injected into the collector due to the forward bias V_{BC}. For $V_{BC} > 0.7$ V (high injection from the B-C junction), a higher fraction of generated hot holes can transit through the narrow base and cross the B-C junction potential barrier, leading to a reversal in the direction of net I_B (see Fig. 3(b)). Similarly, cool electrons injected from the collector can diffuse through the narrow base and enter the E-B space charge region to contribute to avalanche multiplication at a lower V_{EB} (see corresponding TCAD results in Fig. 3). Thus, the likelihood of both hot electrons and hot holes to be coincident is reduced. It is expected that recombination between either hot electrons with cool holes or cool electrons with hot holes near the E-B junction will be more likely and lead to photon-emission with energies in the range 1.5–1.7 eV (λ ~700-800 nm), as predicted in [24].

Figure 4(a) shows the measured $\varepsilon(\lambda)$ of the AMLET, where the intensities are normalized by setting $\int \varepsilon(\lambda) d\lambda = 1$. Effect

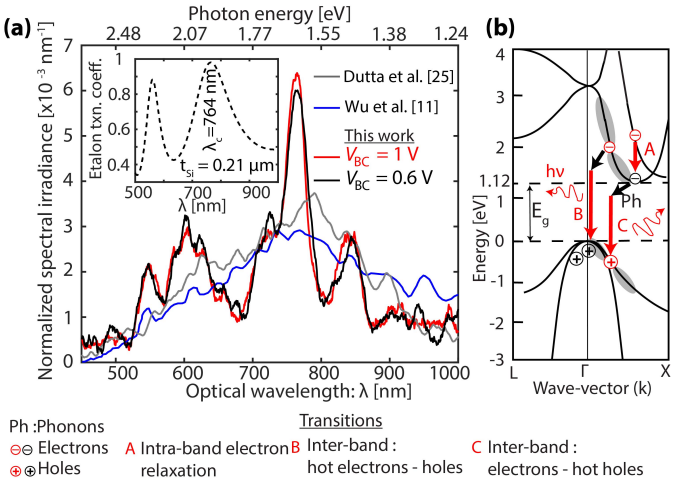

Fig. 4. (a) Normalized EL spectral irradiance of the AMLET (red) measured vertically. Prior reported AM EL-spectra from 2-terminal [25] (grey) and 3-terminal [11] (blue) LEDs in Si CMOS technologies are shown for comparison. (Inset): Calculated spectral transmission coefficient of a 1-D Si Fabry-Pérot resonator (etalon) surrounded by SiO_2 showing a resonance at 764 nm coinciding with the AMLET EL-intensity peak. (b) Schematic E-k diagram of Si illustrating possible pathways for electron transitions that contribute to photon emission. The grey regions indicate the schematic energy ranges of hot carrier distributions reported in [24] and [36].

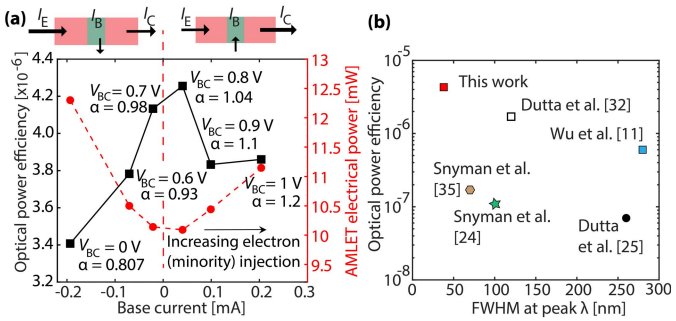

Fig. 5. (a) AMLET optical power efficiency (black symbols) and electrical power (red symbols) at $I_E = 1$ mA for varying I_B. Negative (positive) sign of I_B indicates a current leaving (entering) the terminal, illustrated in the sketch above. A maximum is observed at $V_{BC} = 0.8$ V corresponding to an common-base current gain $\alpha = 1.04$. (b) Benchmark of η_{opt} against FWHM (at the peak λ) of our work.

of varying V_{BC} on $\varepsilon(\lambda)$ is negligible, indicating no effect on carrier energy distributions. We observe three important spectral bands: the yellow (Y)-band near $\lambda \approx 600$ nm, red (R)-band near $\lambda \approx 764$ nm and near-infrared (NIR) band near $\lambda \approx 850$ nm. Fig. 4(b) shows the Si energy dispersion curve (E-k diagram) with possible electron energy transitions used to explain the observed EL. Photon emission in the R-band (photon energies near 1.6 eV) is attributed to phonon-assisted recombination between hot electrons and holes (transition 'B' in Fig. 4(b)). The Y- and NIR band are attributed to other processes [24]. The peak intensity in the R-band is 2 times higher than that of the Y or NIR bands, and the FWHM of the R-band peak is only 38 nm (i.e. quality factor of 20). Such a spectral enhancement is significantly higher than that in prior reported Si AMLEDs [11], [24], [25], [32] (see Fig. 4). Further, the FWHM is, till date, the smallest reported for Si AM light-emitting devices.

The observed $\varepsilon(\lambda)$ depends on both electronic transitions and the optical mode density, and can be attributed to two factors. Firstly, our AMLET design favours photon emission in the R-band as discussed earlier. Secondly, the active Si cavity forms a lossy Fabry-Pérot resonator (etalon) [33] along z-axis. Considering the λ-dependent Fresnel reflection coefficient at the Si-SiO_2 interfaces with normal incidence of light, the Si refractive index (n_{Si}) and extinction coefficient [34], the calculated etalon transmission coefficient exhibits resonances at 764 nm ($\approx n_{Si} \cdot t_{Si}$) and at 560 nm for $t_{Si} = 0.21$ μm (inset of Fig. 4(a)). These agree with the peaks in the EL-spectrum measured within small angles ($\leq$10 deg.) of incidence, including the valley within 650–700 nm. The deviations in the peak and valley locations are likely due to the electronic contribution to $\varepsilon(\lambda)$, not included in the calculation. Note that EL at 560 nm is attributed to processes (transition types A/B in Fig. 4(b)) similar to that in Y-band [24]. For comparison, in 2-terminal AMLEDs excluding FP resonance [32], λ-peaks were reported near 480 nm, 620 nm, and 700 nm; these were governed only by electronic transitions.

The η_{opt} of the AMLET is defined as $P_{opt}/P_{electrical}$, where $P_{electrical} = I_E \cdot V_{EC}$ for $V_{BC} < 0.8$ V and $= I_C \cdot V_{EC}$ for $V_{BC} \geq 0.8$ V. Fig. 5(a) shows that η_{opt} increases with increasing V_{BC}, and reaches a maximum of 4.3×10^{-6} at $V_{BC} = 0.8$ V, while $P_{electrical}$ reaches a minimum. A reversal in the direction of I_B demarcates the transition from low to high injection regimes. For $V_{BC} > 0.8$ V, η_{opt} reduces due to an eventual increase in $P_{electrical}$. Our AMLET, has a device footprint of 420 μm^2, emits a total $P_{opt} = 43$ nW at $P_{electrical} = 10$ mW. Assuming that the light is uniformly emitted from the base region, this translates to an estimated AMLET intensity of 215 mW cm^{-2}. The corresponding P_{opt} estimated around the peak $\lambda = 764$ ($\pm$19 nm) is 8 nW (intensity $\sim$40 mW cm^{-2}). No significant change in $\varepsilon(\lambda)$ and in η_{opt} was observed when the measurements were repeated spanning a continuous operation time of at least $\sim$ 3 hours. Comparison of η_{opt} versus spectral FWHM with those of prior art is shown in Fig. 5(b). The effects of further narrowing of the base region on η_{opt} requires a future study. While a shorter base length would increase the carrier injection, it is also likely to shorten the light-emission region. Further, the impact of varying t_{Si} and temperature on the peak λ and η_{opt} should be investigated. Based on FP theory, a direct relation between peak λ and t_{Si} is expected, while η_{opt} will reduce with temperature due to a positive temperature coefficient [37] in V_{br}.

III. Conclusion

We presented an avalanche-mode light-emitting transistor in a silicon-on-insulator technology. By combining a high injection current density through a narrow base region with Fabry-Pérot optical resonance in the a thin SOI layer, a high optical power efficiency and a low FWHM was achieved.

Acknowledgment

Device fabrication was done by IMEC vzw, Leuven, Belgium.

REFERENCES

[1] R. Newman, "Visible light from a silicon p–n junction," *Phys. Rev.*, vol. 100, no. 2, pp. 700–703, Oct. 1955, doi: 10.1103/PhysRev.100.700.

[2] A. G. Chynoweth and K. G. Mckay, "Photon emission from avalanche breakdown in silicon," *Phys. Rev.*, vol. 102, no. 2, pp. 369–376, Apr. 1956, doi: 10.1103/PhysRev.102.369.

[3] M. D. Plessis, H. Aharoni, and L. W. Snyman, "Silicon LEDs fabricated in standard VLSI technology as components for all silicon monolithic integrated optoelectronic systems," *IEEE J. Sel. Topics Quantum Electron.*, vol. 8, no. 6, pp. 1412–1419, Nov. 2002, doi: 10.1109/JSTQE.2002.806697.

[4] L. W. Snyman, M. D. Plessis, and H. Aharoni, "Injection-avalanche-based n^+pn silicon complementary metal–oxide–semiconductor light-emitting device (450–750 nm) with 2-order-of-magnitude increase in light emission intensity," *Jpn. J. Appl. Phys.*, vol. 46, no. 4, pp. 2474–2480, Apr. 2007, doi: 10.1143/JJAP.46.2474.

[5] B. Huang, X. Zhang, W. Wang, Z. Dong, N. Guan, Z. Zhang, and H. Chen, "CMOS monolithic optoelectronic integrated circuit for on-chip optical interconnection," *Opt. Commun.*, vol. 284, nos. 16–17, pp. 3924–3927, Aug. 2011, doi: 10.1016/j.optcom.2011.04.028.

[6] A. Khanmohammadi, R. Enne, M. Hofbauer, and H. Zimmermann, "Monolithically integrated optical random pulse generator in high voltage CMOS technology," in *Proc. 45th Eur. Solid State Device Res. Conf. (ESSDERC)*, Sep. 2015, pp. 138–141, doi: 10.1109/ESSDERC.2015.7324732.

[7] S. Dutta, V. Agarwal, R. J. E. Hueting, J. Schmitz, and A.-J. Annema, "Monolithic optical link in silicon-on-insulator CMOS technology," *Opt. Exp.*, vol. 25, no. 5, pp. 5440–5456, Mar. 2017, doi: 10.1364/OE.25.005440.

[8] V. Agarwal, S. Dutta, A. J. Annema, R. J. E. Hueting, J. Schmitz, M. J. Lee, E. Charbon, and B. Nauta, "Optocoupling in CMOS," in *IEDM Tech. Dig.*, Dec. 2018, pp. 739–742, doi: 10.1109/IEDM.2018.8614523.

[9] C. Roques-Carmes, S. E. Kooi, Y. Yang, A. Massuda, P. D. Keathley, A. Zaidi, Y. Yang, J. D. Joannopoulos, K. K. Berggren, I. Kaminer, and M. Soljačić, "Towards integrated tunable all-silicon free-electron light sources," *Nature Commun.*, vol. 10, no. 1, pp. 1–8, Jul. 2019, doi: 10.1038/s41467-019-11070-7.

[10] S. W. Schmitt, K. Schwarzburg, G. Sarau, S. H. Christiansen, S. Wiesner, and C. Dubourdieu, "All-silicon polarized light source based on electrically excited whispering gallery modes in inversely tapered photonic resonators," *APL Mater.*, vol. 8, no. 6, Jun. 2020, Art. no. 061110, doi: 10.1063/5.0007759.

[11] K. Wu, H. Zhang, Y. Chen, Q. Luo, and K. Xu, "All-silicon microdisplay using efficient hot-carrier electroluminescence in standard 0.18 μm CMOS technology," *IEEE Electron Device Lett.*, vol. 42, no. 4, pp. 541–544, Apr. 2021, doi: 10.1109/LED.2021.3059781.

[12] S. Y. Siew, B. Li, F. Gao, H. Y. Zheng, W. Zhang, P. Guo, S. W. Xie, A. Song, B. Dong, L. W. Luo, C. Li, X. Luo, and G.-Q. Lo, "Review of silicon photonics technology and platform development," *J. Lightw. Technol.*, vol. 39, no. 13, pp. 4374–4389, Jul. 2021, doi: 10.1109/JLT.2021.3066203.

[13] B. P. van Drieenhuizen and R. F. Wolffenbuttel, "Optocoupler based on the avalanche light emission in silicon," *Sens. Actuators A, Phys.*, vol. 31, pp. 229–240, Mar. 1992, doi: 10.1016/0924-4247(92)80110-O.

[14] M. Ramamurthy and V. Lakshminarayanan, "Human vision and perception," in *Handbook of Advanced Lighting Technology*, R. Karlicek, C. C. Sun, G. Zissis, and R. Ma, Eds. Cham, Switzerland: Springer, Mar. 2015, doi: 10.1007/978-3-319-00295-8_46-1.

[15] H. Croft and J. M. Chen, "Leaf pigment content," in *Comprehensive Remote Sensing*, vol. 3, S. Lian, Ed. Amsterdam, The Netherlands: Elsevier, 2018, ch. 9, pp. 117–142, doi: 10.1016/B978-0-12-409548-9.10547-0.

[16] L. Li, A. A. Shemetov, M. Baloban, P. Hu, L. Zhu, D. M. Shcherbakova, R. Zhang, J. Shi, J. Yao, L. V. Wang, and V. V. Verkhusha, "Small near-infrared photochromic protein for photoacoustic multi-contrast imaging and detection of protein interactions *in vivo*," *Nature Commun.*, vol. 9, no. 1, p. 2734, Jul. 2018, doi: 10.1038/s41467-018-05231-3.

[17] S. K. Lazarouk, A. A. Leshok, T. A. Kozlova, A. V. Dolbik, L. D. Vi, V. K. Ilkov, and V. A. Labunov, "3D silicon photonic structures based on avalanche LED with interconnections through optical interposer," *Int. J. Nanoscience*, vol. 18, Jun. 2019, Art. no. 1940091, doi: 10.1142/S0219581X1940091X.

[18] S. Dutta, P. G. Steeneken, and G. J. Verbiest, "Optical sensing of chlorophyll (in) with dual-spectrum Si LEDs in SOI-CMOS technology," *IEEE Sensors J.*, vol. 22, no. 12, pp. 11280–11289, Jun. 2022, doi: 10.1109/JSEN.2021.3086588.

[19] V. Agarwal, S. Dutta, A.-J. Annema, R. J. Hueting, P. G. Steeneken, and B. Nauta, "Low power wide spectrum optical transmitter using avalanche mode LEDs in SOI CMOS technology," *Opt. Exp.*, vol. 25, no. 15, pp. 16981–16995, Jul. 2017, doi: 10.1364/OE.25.016981.

[20] M. O'Toole, K. T. Lau, R. Shepherd, C. Slater, and D. Diamond, "Determination of phosphate using a highly sensitive paired emitter–detector diode photometric flow detector," *Analytica Chim. Acta*, vol. 597, no. 2, pp. 290–294, Aug. 2007, doi: 10.1016/j.aca.2007.06.048.

[21] M. O'Toole and D. Diamond, "Absorbance based light emitting diode optical sensors and sensing devices," *Sensors*, vol. 8, no. 4, pp. 2453–2479, Apr. 2008, doi: 10.3390/s8042453.

[22] P. Yeh, N. Yeh, C.-H. Lee, and T.-J. Ding, "Applications of LEDs in optical sensors and chemical sensing device for detection of biochemicals, heavy metals, and environmental nutrients," *Renew. Sustain. Energy Rev.*, vol. 75, pp. 461–468, Aug. 2017, doi: 10.1016/j.rser.2016.11.011.

[23] L. W. Snyman, K. Xu, J.-L. Polleux, K. A. Ogudo, and C. Viana, "Higher intensity SiAvLEDs in an RF bipolar process through carrier energy and carrier momentum engineering," *IEEE J. Quantum Electron.*, vol. 51, no. 7, Jul. 2015, Art. no. 3200110, doi: 10.1109/JQE.2015.2427036.

[24] L. W. Snyman, K. Xu, and J.-L. Polleux, "Micron and nano-dimensioned silicon LEDs emitting at 650 and 750–850 nm wavelengths in standard Si integrated circuitry," *IEEE J. Quantum Electron.*, vol. 56, no. 4, Aug. 2020, Art. no. 3200210, doi: 10.1109/JQE.2020.2994980.

[25] S. Dutta, P. G. Steeneken, V. Agarwal, J. Schmitz, A.-J. Annema, and R. J. E. Hueting, "The avalanche-mode superjunction LED," *IEEE Trans. Electron Devices*, vol. 64, no. 4, pp. 1612–1618, Apr. 2017, doi: 10.1109/TED.2017.2669645.

[26] K. Xu and G. P. Li, "A three-terminal silicon-PMOSFET-like light-emitting device (LED) for optical intensity modulation," *IEEE Photon. J.*, vol. 4, no. 6, pp. 2159–2168, Dec. 2012, doi: 10.1109/JPHOT.2012.2224101.

[27] P. P. Absil, P. De Heyn, H. Chen, P. Verheyen, G. Lepage, M. Pantouvaki, J. De Coster, A. Khanna, Y. Drissi, D. Van Thourhout, and J. Van Campenhout, "Imec iSiPP25G silicon photonics: A robust CMOS-based photonics technology platform," in *Proc. SPIE*, vol. 9367, Feb. 2015, Art. no. 93670V, doi: 10.1117/12.2076262.

[28] T. H. Ning, "A perspective on SOI symmetric lateral bipolar transistors for ultra-low-power systems," *IEEE J. Electron Devices Soc.*, vol. 4, no. 5, pp. 227–235, Sep. 2016, doi: 10.1109/JEDS.2016.2528119.

[29] *ATLAS Device Simulation Software*, V. 5.30.0.R, Silvaco, Santa Clara, CA, USA, 2020.

[30] T. Grasser, H. Kosina, C. Heitzinger, and S. Selberherr, "Accurate impact ionization model which accounts for hot and cold carrier populations," *Appl. Phys. Lett.*, vol. 80, no. 4, pp. 613–615, Jan. 2002, doi: 10.1063/1.1445273.

[31] J.-B. Yau, J. Cai, P. Hashemi, K. Balakrishnan, C. D'Emic, and T. H. Ning, "A study of process-related electrical defects in SOI lateral bipolar transistors fabricated by ion implantation," *J. Appl. Phys.*, vol. 123, no. 16, Apr. 2018, Art. no. 161526, doi: 10.1063/1.5001203.

[32] S. Dutta, G. J. M. Wienk, R. J. E. Hueting, J. Schmitz, and A.-J. Annema, "Optical power efficiency versus breakdown voltage of avalanche-mode silicon LEDs in CMOS," *IEEE Electron Device Lett.*, vol. 38, no. 7, pp. 898–901, Jul. 2017, doi: 10.1109/LED.2017.2701505.

[33] K. F. Renk, "Fabry–Perot resonator," in *Basics of Laser Physics*. Berlin, Germany: Springer, 2012, ch. 3, pp. 43–54, doi: 10.1007/978-3-642-23565-8_3.

[34] M. A. Green, "Self-consistent optical parameters of intrinsic silicon at 300K including temperature coefficients," *Sol. Energy Mater. Sol. Cells*, vol. 92, no. 11, pp. 1305–1310, Nov. 2008, doi: 10.1016/j.solmat.2008.06.009.

[35] L. W. Snyman, J.-L. Polleux, M. D. Plessis, and K. A. Ogudo, "Stimulating 600–650 nm wavelength optical emission in monolithically integrated silicon LEDs through controlled injection-avalanche and carrier density balancing technology," *IEEE J. Quantum Electron.*, vol. 53, no. 5, Oct. 2017, Art. no. 7100209, doi: 10.1109/JQE.2017.2736254.

[36] L. W. Snyman, M. D. Plessis, and E. Bellotti, "Photonic transitions (1.4 eV–2.8 eV) in silicon p^+np^+ injection-avalanche CMOS LEDs as function of depletion layer profiling and defect engineering," *IEEE J. Quantum Electron.*, vol. 46, no. 6, pp. 906–919, Jun. 2010, doi: 10.1109/JQE.2009.2036746.

[37] R. van Overstraeten and H. de Man, "Measurement of the ionization rates in diffused silicon p–n junctions," *Solid-State Electron.*, vol. 13, no. 1, pp. 583–608, May 1970, doi: 10.1016/0038-1101(70)90139-5.